Volume 11
Number 26
14 July 2023
Pages 13797–14434

Journal of Materials Chemistry A

Materials for energy and sustainability

rsc.li/materials-a

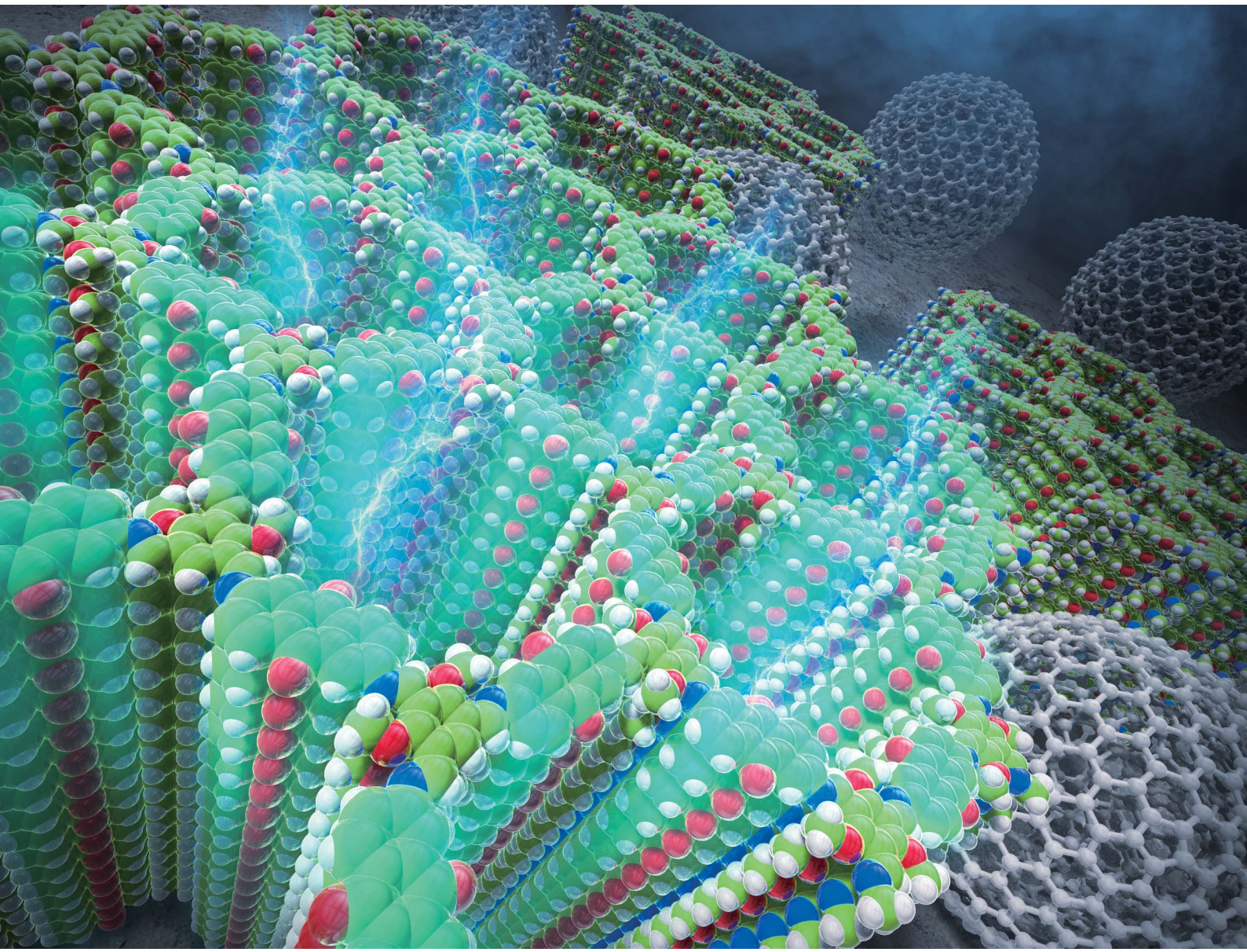

ISSN 2050-7488

ROYAL SOCIETY OF CHEMISTRY

PAPER

Kouki Oka, Norimitsu Tohnai, Rikard Emanuelsson *et al.*
Redox-site accessibility of composites containing a 2D redox-active covalent organic framework: from optimization to application

10 YEARS ANNIVERSARY

Journal of Materials Chemistry A

ROYAL SOCIETY OF CHEMISTRY

PAPER

View Article Online
View Journal | View Issue

Check for updates

Cite this: J. Mater. Chem. A, 2023, 11, 13923

Redox-site accessibility of composites containing a 2D redox-active covalent organic framework: from optimization to application†‡

Tyran Günther,[a] Kouki Oka, *[b] Sandra Olsson, [a] Michelle Åhlén,[a] Norimitsu Tohnai*[b] and Rikard Emanuelsson *[c]

Redox-active covalent organic frameworks (RACOFs) can be employed in various functional materials and enesrgy applications. A crucial performance or efficiency indicator is the percentage of redox centres that can be utilised. Herein, the term redox-site accessibility (RSA) is defined and shown to be an effective metric for developing and optimising a 2D RACOF (*viz.*, TpOMe-DAQ made from 2,4,6-trimethoxy-1,3,5-benzenetricarbaldehyde [TpOMe] and 2,6-diaminoanthraquinone [DAQ]) as an anode material for potential organic-battery applications. Pristine TpOMe-DAQ utilises only 0.76% of its redox sites, necessitating the use of conductivity-enhancement strategies such as blending it with different conductive carbons, or performing *in situ* polymerisation with EDOT (3,4-ethylenedioxythiophene) to form a conductive polymer. While conductive carbon-RACOF composites showed a modest RSA improvement of 4.0%, conductive polymer-RACOF composites boosted the redox-site usage (RSA) to 90% at low mass loadings. The material and electrochemical characteristics of the conductive polymer-RACOF composite containing more-than-necessary conductive polymer showed a reduced surface area but almost identical electrochemical behaviour, compared to the optimal ratio. The high RSA of the optimally loaded composite was replicated in a RACOF-air battery with over 90% active redox sites. We believe that the reported approach and methods, which can be employed on a milligram scale, could serve as a general guide for the electrification and characterisation of RACOFs, as well as for other redox-active porous polymers.

Received 24th January 2023
Accepted 13th April 2023

DOI: 10.1039/d3ta00422h

rsc.li/materials-a

Open Access Article. Published on 13 April 2023. Downloaded on 7/30/2025 3:06:44 AM.
This article is licensed under a Creative Commons Attribution 3.0 Unported Licence.

Introduction

Two-dimensional covalent organic frameworks (2D COFs) are typically porous and microcrystalline materials made up of covalently-bonded atomic layers, which are stacked on top of each other and held in place by non-covalent interactions.[1] Each layer is constructed under reversible bond-forming conditions from monomers possessing restricted bonding directions. Once connected, they form the extended and repeatable covalent bonding pattern that defines the framework.[1,2] When one of these monomers is deliberately selected/tailored to possess a reversible redox-active functional group (which can be accessed within a reasonable and application-specific voltage window), redox-active COFs (RACOFs) can be formed.[3] Such layered 2D RACOFs have been investigated as functional materials for applications in various technologies: energy storage devices (Li-ion batteries[4–8] and pseudocapacitors[9]), electrocatalysis,[10] reductive ion-trapping,[11,12] and chemical sensing.[13] Accessing as many redox sites as possible in a material is of considerable importance, because the theoretical capacity of batteries, efficiency of electrocatalysts, and sensitivity of sensors (which are all headline material characteristics) depend on the number of redox sites that can be utilised. Therefore, mapping a functional material's application-specific limitations is crucial for both fundamental understanding and achieving optimised performance.[14]

For ease of description, we here employ the term "redox-site accessibility" (RSA) and clearly define its meaning throughout this article. In the context of a material that contains a known number of potential redox sites, RSA is a metric in percent and is meant to represent the percentage of redox sites inferred

[a]Nanotechnology and Functional Materials, Department of Materials Science and Engineering, The Ångström Laboratory, Uppsala University, Box 35, SE-751 03 Uppsala, Sweden

[b]Center for Future Innovation (CFi) and Department of Applied Chemistry, Graduate School of Engineering, Osaka University, 2-1 Yamadaoka, Suita, Osaka 565-0871, Japan. E-mail: oka@chem.eng.osaka-u.ac.jp; tohnai@chem.eng.osaka-u.ac.jp

[c]Department of Chemistry – BMC, Uppsala University, Box 576, SE-751 23 Uppsala, Sweden. E-mail: rikard.emanuelsson@kemi.uu.se

† When applying the BET method, IUPAC recommends interpreting the calculated surface area as an apparent surface area, especially for porous materials that show a combination of type 1 and type 2 isotherms.[38] The term BET-area has been used instead of BET surface area to discourage the reader from assuming the values represent accurate surface areas. The term "specific BET-area" used herein means the apparent surface area per gram of material.

‡ Electronic supplementary information (ESI) available. See DOI: https://doi.org/10.1039/d3ta00422h

Open Access Article. Published on 13 April 2023. Downloaded on 7/30/2025 3:06:44 AM. This article is licensed under a Creative Commons Attribution 3.0 Unported Licence.

based on the experimentally observed faradaic charge from an application-specific measurement (*i.e.*, faradaic charge measured/theoretically expected faradaic charge × 100). The term "redox-site accessibility" has been previously defined and used in context of conducting polymers.[15] This metric is both convenient and crucial in accounting for how efficiently the redox sites in the material are utilised. In addition, comparing and evaluating RSA values for different materials and composites offers the possibility of assisting in guiding their rational improvement.

Although many bulk 2D RACOFs have demonstrated a significantly reduced ability to store and release electrons at their redox sites (*i.e.*, they have low RSA), thin films (up to a few hundred nm) have shown better characteristics (higher RSA).[9,16] Owing to the highly porous structures of most 2D RACOFs (whereby ion diffusion is not expected to be limiting),[17] the problem of low RSA has mainly been attributed to poor electron conductivity throughout the material.[9]

Consequently, this problem has been tackled by several strategies, mostly involving the production of composite materials. The first approach, which has long been customary in electrode preparation, is simply mixing the 2D RACOF material with a chosen amount and type of conductive carbon.[10,18,19] A second approach involves polymerizing the 2D RACOF in the presence of conductive carbon, consequently forming thin films over the surface of conductive carbon structures.[4,8,19] The third approach involves infusing the 2D RACOFs with specific monomers that could subsequently form a conductive polymer (*e.g.*, poly(3,4-ethylenedioxythiophene), PEDOT) *via* electropolymerisation,[16] chemical oxidation,[6,16] or heating.[20] Regarding this third approach, polymerisation *via* chemical oxidation or heating (as with the solid-state polymerisation of 2,5-dibromo-3,4-ethylenedioxythiophene) offers the advantage of producing a ready-to-use powder on large scales compared with the production method of electropolymerisation.[21]

In Dichtel *et al.*'s pioneering work on boosting redox-site accessibility in a 2D RACOF with anthraquinone redox units, they emphasised that adding more than the necessary conducting polymer to the RACOF would ultimately reduce the gravimetric capacity of the composite material, and they allude to the potential benefits of optimising this parameter.[6,16] Furthermore, the addition of a conducting polymer into porous materials *via* monomer infusion has been shown to reduce the material's specific Brunauer–Emmett–Teller (BET) area and porosity,[20,22,23] as well as affect the material's conductivity (wherein adding more polymer improved electronic transport).[22,23] These studies suggest a trade-off between conductivity and material porosity at high loadings which could affect the electrochemical performance of redox-active materials that rely on efficient mass transport.

Here, we aim to map RSA in a porous 2D RACOF and reveal if the material's apparent high surface area or key electrochemical parameters undergo a trade-off at higher conducting-additive loadings. Marder and co-workers recently reported on a structure–property relationship between a microcrystalline 2D RACOF, its amorphous 1D and 2D analogues and their respective electrochemical performance.[24] Their study revealed (by varying the redox-active polymer's structure while keeping the conductive additive constant) the best choice of redox-active polymer structure for an electrochemical device was not straightforward as both 1D amorphous and 2D COF polymers performed well. Here, we report a complementary study where the redox-active polymer's structure is kept constant while the conductive additive is varied. We report a rational and systematic method for electrifying 2D RACOFs, characterising the resulting composite, evaluating its electrochemistry, and employing it as a functional material. Starting from commercial carbons, we demonstrated how the RSA metric could guide rational improvement of the material and emphasised the dramatic improvement using *in situ* formation of PEDOT. Furthermore, we show how the amount of conductive additive affects the RSA, surface area, material porosity and resulting electrochemistry. Finally, we employed the optimised composite as the active anodic component in a promising RACOF-air battery that exhibited excellent performance. The methodology employed might also apply to other porous polymers containing redox-active units, and we believe that it can serve as a general guide for the electrification and characterisation of such materials.

Results and discussion

We chose TpOMe-DAQ[25] (made from 2,4,6-trimethoxy-1,3,5-benzenetricarbaldehyde [TpOMe] and 2,6-diaminoanthraquinone [DAQ]) as our 2D RACOF model for redox-site accessibility (RSA) studies and low-potential anodic material (for the battery application) because it can undergo a reversible $2e^-/2H^+$ anthraquinone/hydroanthraquinone redox reaction (see Fig. S1 in the ESI‡). Its attractive properties include demonstrated stability in aqueous acid/base solutions and a high average specific BET-area (~1530 $m^2\ g^{-1}$ compared to 1120 $m^2\ g^{-1}$ for the more studied analogue, DAAQ-TFP[18]).

The four-step synthesis of TpOMe from 1,3,5-trimethoxybenzene was performed according to the strategy first outlined by Banerjee *et al.*[26] (ESI‡ Section 2 describes each synthesis step and highlights where any modifications were made). The prepared COF material was characterised using powder X-ray diffraction (PXRD), N_2 sorption isotherms, Fourier transform infrared (FT-IR) spectroscopy, scanning electron microscopy with energy dispersive analysis (SEM-EDX), thermogravimetric analysis (TGA) and elemental analysis (EA). The specific BET-area (1574 ± 14 *vs.* 1530 $m^2\ g^{-1}$), pore size distribution (2.1 *vs.* 2.4 nm), PXRD peaks and FT-IR for our TpOMe-DAQ were all in excellent agreement with previous reports (see ESI‡ Section 5.1 for details).[25] The PXRD and the large specific BET-area indicate the COF is mostly microcrystalline, however, we cannot determine with certainty how much of the material is crystalline or amorphous nor how these regions are distributed throughout the material. Both EA and SEM-EDX confirmed the presence of small amounts of residual sulphur in the TpOMe-DAQ, which originated from the excess *para*-toluenesulphonic acid (PTSA) used during the synthesis (ESI Table S2 and Fig. S18‡). However, extensive washing and sonication can reduce this amount. Particle size measurements using laser

 This journal is © The Royal Society of Chemistry 2023

Open Access Article. Published on 13 April 2023. Downloaded on 7/30/2025 3:06:44 AM.
This article is licensed under a Creative Commons Attribution 3.0 Unported Licence.

diffraction suggested that particle aggregates ranged from approximately 2 to 350 μm in size, with most aggregates distributed around 20 and 80 μm (ESI Fig. S19‡).

In a functional material designed to incorporate redox-active molecular units, the number of accessible centres is a crucial parameter. For example, the faradaic charge (typically originating from these accessible redox-sites within the electrode material), mainly determines the battery's capacity during cycling.[27] We investigated pristine TpOMe-DAQ together with only PVDF as a binder (10% of the combined mass) to establish a baseline, that is, to determine how many redox units could be electrochemically accessed in the pristine material and to establish whether conductive additives would be required. To allow for upscaling, the focus was on higher material loadings beyond very thin and ordered films. A mass loading between 0.45 to 0.75 mg cm^{-2} formed evenly-coated films, and produced reasonably reproducible (std = 0.06%) RSA values of *ca.* 0.76% when utilizing an aqueous acidic electrolyte and determining the faradaic charge from three-electrode cyclic voltammetry (see ESI‡ Sections 1.10 and 3 for all details). This suggests that only 1 in every 130 redox-active sites within the TpOMe-DAQ framework is electrochemically accessible and such low RSA has previously been attributed to poor electron conductivity in similar framework materials.[9] It should be noted that the method used here to evaluate RSA cannot distinguish between redox-active moieties located in crystalline or amorphous domains within the COF material. It also assumes an infinite and defect-free repetition of the redox moiety depicted in Fig. S17.‡ We also observed that lower areal loading, of the TpOMe-DAQ and PVDF mixture, showed higher RSA values while loading above 0.75 mg cm^{-2} showed decreasing RSA values (ESI Section 4.1 and Fig. S8‡). This trend is expected for a material that exhibits poor framework and interparticle conductivity, whereby only the tiny fraction of redox-active sites on the surface of particles directly contacting the current collector have a conducting pathway.

Clearly, conductive additives are needed in order to attempt to improve the RSA. The go-to material used to achieve this is conductive carbon which is commonly used to ensure material conductivity in the fabrication of battery electrodes. Conductive carbon has several benefits, as it is inherently conductive at all electronic potentials, chemically very stable, and exists in a range of forms as well as being readily available.[28] It should be noted that the addition of conductive additives increases the mass of the composite blend without adding redox-active sites, and therefore results in a reduced gravimetric capacity for the composite, which is negative in, for example, battery applications. The effect of increasing the C : TpOMe-DAQ mass ratio on the RSA of TpOMe-DAQ was explored, and the results are shown in Fig. 1A. Blending pristine TpOMe-DAQ with conductive carbon (see ESI‡ Section 3 for methods and 4.2, for further details) improved its RSA from 0.76% to 3.4%, but not indefinitely for higher C : TpOMe-DAQ ratios (indicated by a plateau in Fig. 1A). The onset of the plateau was observed at 25% carbon in the blend (corresponding to a C : TpOMe-DAQ mass ratio of approximately 0.38). More carbon added very little to the RSA of the active material and instead reduced the composite's

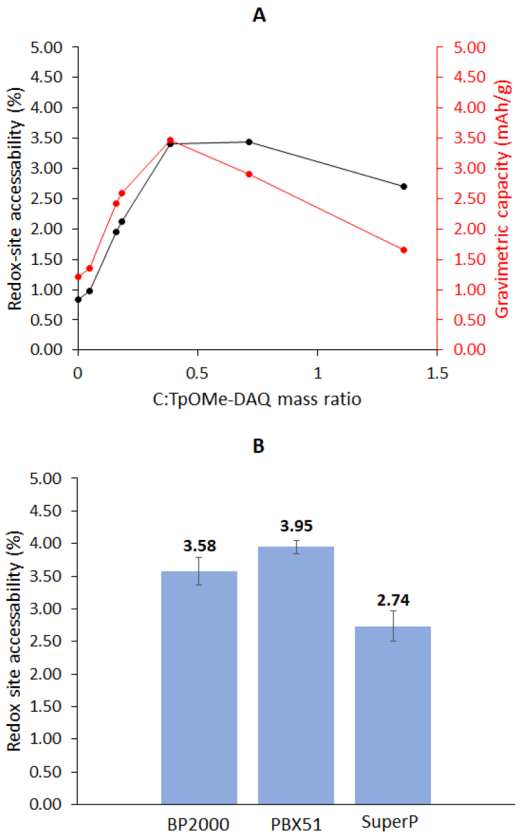

Fig. 1 The effects of the amount (A) and type of conductive carbon (B) on TpOMe-DAQ's redox-site accessibility. (A) The amount of BP2000 was increased relative to the amount of TpOMe-DAQ and defined by the C : COF (mass/mass) ratio. The COF's RSA (black) and composite's gravimetric capacity (red) excluding the PVDF binder were evaluated. (B) The RSA of TpOMe-DAQ was evaluated at the mass ratio of 0.38C : TpOMe-DAQ with different conductive carbon types (BP2000, PBX51, and SuperP) in triplicate and their relative standard deviations are represented by the black error bars.

gravimetric capacity unnecessarily by adding weight without activating more redox sites (note that any capacitance originating from the carbon additive is excluded in the capacity calculation, see ESI‡ Section 3).

For redox-active materials that exhibit poor interparticle conductivity, blending them with conductive carbon would be expected to improve their RSA values owing to better accessibility of the surface redox-active groups in all the particles within the film (and not just those contacting the current collector). This should also enable higher areal loading without forfeiting the RSA. Such an observation was in fact made when more than doubling the areal loading (from 0.70 to 1.67 mg cm^{-2}) in a 25% BP2000 (Cabot Corporation) blend with TpOMe-DAQ did not reduce its RSA to any degree outside of experimental error. Furthermore, the effect of the conductive-carbon type (BP2000, PBX51 and SuperP were chosen because they possess different characteristics[29]) on the RSA of TpOMe-DAQ was evaluated at a C : TpOMe-DAQ mass ratio of 0.38 in triplicate (Fig. 1B). For the electrode blend containing 65% TpOMe-DAQ, 25% conductive carbon and 10% PVDF binder,

Open Access Article. Published on 13 April 2023. Downloaded on 7/30/2025 3:06:44 AM.
This article is licensed under a Creative Commons Attribution 3.0 Unported Licence.

TpOMe-DAQ exhibited the highest RSA of 4.0% when PBX51 was used. The magnitude of the standard deviation bars for these results also provides insight into the reliability of the method used to obtain RSA values.

The above findings show that in poorly conductive 2D RACOFs, only modest improvements can be achieved by blending them post-synthetically with conductive carbons, and that the primary benefit of such blending is to enable higher areal loading without further reducing their RSA values (owing to the poor contact with particles further away from the current collector). It should be noted however, that high RSA values have been reported for some 2D-RACOFs blended with conductive carbon.[24]

Improved electronic conductivity and increased capacity/capacitance in 2D RACOFs have previously been demonstrated by infusing them with monomers of a conducting polymer (followed by *in situ* oxidation either chemically[6,16,20] or electrochemically[16] to form the conducting polymer). As the chemical oxidation approach might offer scalability advantages, we sought to evaluate the effect of the loading amount of EDOT (3,4-ethylenedioxythiophene, the monomer of the conducting polymer PEDOT) on the RSA of TpOMe-DAQ after chemical oxidation (using $FeTs_3 \cdot 6H_2O$). Previous studies have indicated that the half-wave potential of the anthraquinone redox reaction is higher than the conductivity-onset potential of PEDOT in acidic aqueous electrolytes.[16] Selecting a conducting polymer which has a lower conductivity-onset potential (the potential at which the conducting polymer starts oxidizing and consequently becomes conductive) with respect to the redox-active moieties is a general rule and constitutes what is called a "redox match". Without such a redox match, the conducting polymer should not be able to function as a conductive additive. In other words, it would neither enhance the electronic conductivity of the material nor activate redox sites in the potential region of interest.[30,31] Thus, employing a conducting polymer as a conductive additive requires judicious selection of redox groups, conducting polymers and electrolyte/solvent systems. Evaluating potential-dependent conductivity using interdigitated array (IDA) electrodes and a bipotentiostat represents an excellent method to achieve this (*vide infra*).

Explorative synthesis of new materials often results in limitations in the quantities initially produced. Thus, a small-scale method requiring only 1–2 mg of COF material was devised to explore several EDOT : TpOMe-DAQ (mass/mass) loading ratios (see ESI‡ Section 2.4.1). Screening demonstrated that the poor RSA of pristine TpOMe-DAQ and C : TpOMe-DAQ could be dramatically enhanced from 0.76% and 4.0%, respectively, to over 90% by *in situ* EDOT polymerisation. The black line in Fig. 2A shows how gradually increasing the EDOT loading in the composite rapidly activates redox sites, and that a plateau is reached at an EDOT : TpOMe-DAQ mass loading as low as ~0.3. Interestingly, increasing EDOT loading above this ratio only reduced the gravimetric capacity of the material (Fig. 2A, red line), and the remaining ~10% could not be reached. The primary control measurement (no EDOT added) confirmed that the chemical oxidant ($FeTs_3 \cdot 6H_2O$) had no positive effect on the RSA of TpOMe-DAQ (0.76%). Furthermore, a secondary control,

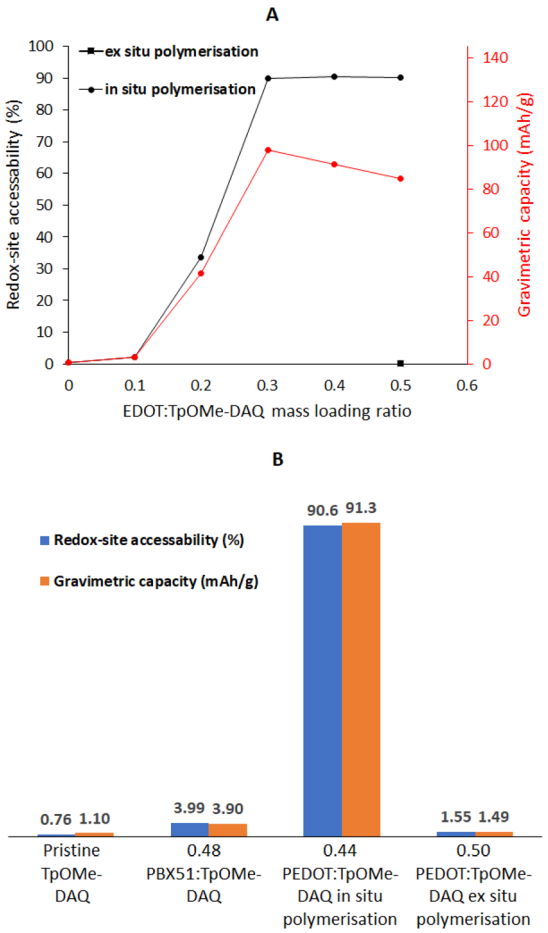

Fig. 2 Depicts how the EDOT : COF mass loading ratio (A) and general conductivity-enhancement method (B) affects TpOMe-DAQ's RSA and the composite's gravimetric capacity. (A) The top of the red *x*-axis is the maximum theoretical capacity for pristine TpOMe-DAQ (144.7 mA h g^{-1} and assumes no added capacity from the conductive additive). "*In situ*" polymerisation implies that EDOT was polymerised in the presence of TpOMe-DAQ in the same tube. "*Ex situ*" polymerisation implies EDOT was first polymerised in a separate tube and then added to TpOMe-DAQ.

where EDOT was polymerised ex situ from TpOMe-DAQ using $FeTs_3 \cdot 6H_2O$ and then blended, demonstrated that EDOT polymerisation in the presence of TpOMe-DAQ was necessary to enhance its RSA because it displayed worse results (RSA = 1.55%) than mixing with carbon. Fig. 2B summarises how the different composite-blending strategies affected the RSA of TpOMe-DAQ and shows the corresponding gravimetric capacity of each composite.

After exploring the effect of different EDOT : TpOMe-DAQ mass loading ratios on the RSA of TpOMe-DAQ, the small-scale method (used for initial screening) was scaled up to produce hundreds of milligrams of 0.2, 0.4, and 0.8 EDOT : TpOMe-DAQ (mass/mass) composite material for further material characterisation. A batch of PEDOT : Ts (PEDOT with *p*-toluenesulfonate anions as dopant) was also synthesised using the same polymerisation conditions as for the composites (but without any TpOMe-DAQ present), which acted as a control for

 This journal is © The Royal Society of Chemistry 2023

Open Access Article. Published on 13 April 2023. Downloaded on 7/30/2025 3:06:44 AM.
This article is licensed under a Creative Commons Attribution 3.0 Unported Licence.

all subsequent characterisation analyses (ESI Scheme S1 and Section 2.3‡). The actual composition of the composites (the relative mass percentages of PEDOT : Ts and TpOMe-DAQ) was evaluated using two methods: the initial-mass method and the EA-XPS method (see ESI‡ Sections 2.4.2 and 5 for details). Both methods yielded composite compositions within ±6% of each other (ESI Table S1‡). XPS of S 2p also suggested that the PEDOT : Ts component of all composites was doped at a 1 : 6 ratio of tosylate anion:PEDOT monomer units.

An overlay of the thermogravimetric (TG) profiles of pristine TpOMe-DAQ, PEDOT : Ts, and 0.4EDOT@TpOMe-DAQ (Fig. 3) demonstrated a two-component composite with PEDOT : Ts decomposing rapidly at 300 °C (Fig. 3A, blue line). After complete combustion at 400 °C, the TG profile of 0.4EDOT@TpOMe-DAQ (green) returned to that of the more stable TpOMe-DAQ COF (orange), indicating that the thermal stability of the composites was limited by that of the PEDOT : Ts component. All the composites, including the PEDOT : Ts control, left a slight red combustion residue presumed to be iron oxide. It was suspected that this originated from the $FeTs_3 \cdot 6H_2O$ oxidant used during the polymerisation of EDOT. An EDS-SEM map of PEDOT : Ts (ESI Fig. S25‡) shows that iron was randomly distributed throughout the polymer and likely to have been trapped during particle aggregation. Based on the TGA analysis and assuming that the red residue was Fe_2O_3, the PEDOT : Ts component of the composites was expected to contain less than 0.85% Fe.

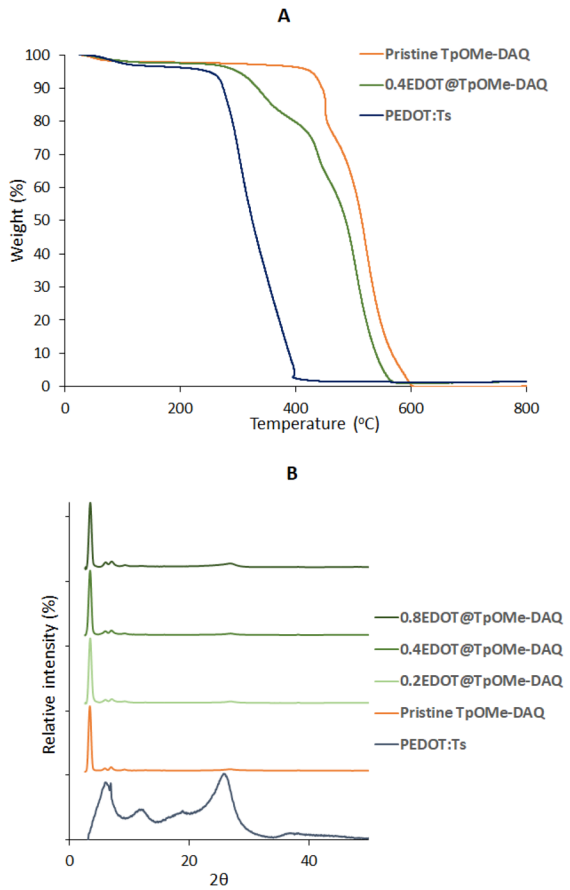

Fig. 3 Overlay plots of air-combustion thermogravimetric profiles for pristine TpOMe-DAQ, 0.4EDOT@TpOMe-DAQ and ex situ polymerized PEDOT : Ts (A) and PXRD diffractograms for the series of *in situ* polymerized composites (B).

The PXRD pattern of the PEDOT control suggested that it was predominantly amorphous, whereas the diffractograms obtained for the composites showed the same pattern as that of pristine TpOMe-DAQ (Fig. 3B). The degree of crystallinity could not be reliably determined from the PXRD patterns. However, it was concluded that the microcrystallinity of TpOMe-DAQ was preserved, and that the polymerisation process likely did not significantly disturb this order.

When comparing the SEM images of pristine TpOMe-DAQ COF (ESI Fig. S18‡) with those obtained for the 0.4EDOT@TpOMe-DAQ composite (ESI Fig. S30‡), the *in situ* polymerisation procedure produced a cauliflower-like coating (presumably PEDOT : Ts) over the different morphological structures of TpOMe-DAQ. A sulphur-rich EDX map (ESI Fig. S30‡) of the imaged composite further supports the formation of an intimate and evenly distributed PEDOT : Ts coating on the surface of the TpOMe-DAQ COF.

The specific BET-area and cumulative pore volume (extracted from Fig. 4A and B, respectively) gradually decreased for composites with higher EDOT loading [pristine TpOMe-DAQ (1574 $m^2\ g^{-1}$), 0.2EDOT@TpOMe-DAQ (1155 $m^2\ g^{-1}$), 0.4EDOT@TpOMe-DAQ (956 $m^2\ g^{-1}$) and 0.8EDOT@TpOMe-DAQ (557 $m^2\ g^{-1}$)]. As both these metrics are evaluated per gram of material, a decrease in their magnitude is expected owing to the addition of more PEDOT : Ts mass in the composites. However, the measured specific BET-areas and cumulative pore volumes of all the composites were lower than expected based on correlating the control measurements with their final mass-measured ratios after synthesis (ESI‡ Section 5.6). These lower-than-expected values suggest that higher EDOT loading blocked a higher percentage of TpOMe-DAQ pores. However, an overlay of the pore-size distribution plots for the different composites (Fig. 4B) showed no evidence of a decrease in pore diameter, which suggests that the PEDOT : Ts surface coating may simply block the probe molecule's access to the pores during measurements.

Dichtel *et al.* and others have previously attributed the enhanced capacity of their composites to PEDOT formation inside the COF pores.[16,20] Herein, the high RSA value (90%) obtained for the *in situ* polymerisation of EDOT *versus* blending TpOMe-DAQ with *ex situ* polymerised PEDOT : Ts (RSA = 1.55%) fits well with the explanation of in-pore PEDOT formation. However, apart from this observation, we could not confidently confirm that PEDOT : Ts had formed within the pores of TpOMe-DAQ using the experimental techniques at hand. The enhanced RSA of TpOMe-DAQ, observed when EDOT was polymerised *in situ*, may have resulted from an intimate surface coating of its particles and not necessarily from creating a conductive network within its pore space.

Next, we evaluated whether loading more than the necessary polymer (which did not activate any more redox sites) into the composite affected the electrochemical performance of the material using an aqueous acidic electrolyte (0.5 M *para-*

Open Access Article. Published on 13 April 2023. Downloaded on 7/30/2025 3:06:44 AM.
This article is licensed under a Creative Commons Attribution 3.0 Unported Licence.

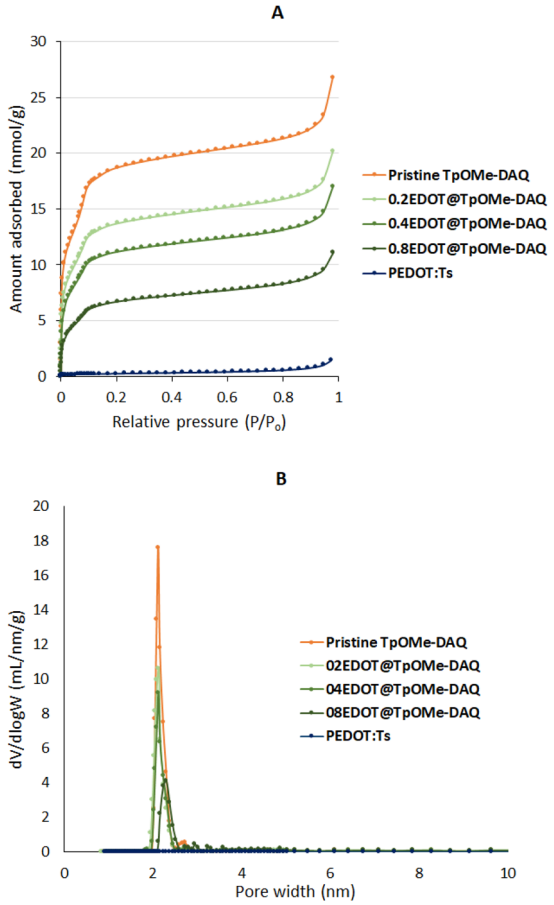

Fig. 4 Overlay plots of N_2 adsorption profiles (A) and their corresponding pore-size distributions (B) for the *in situ* EDOT polymerized series as well as the pristine TpOMe-DAQ and *ex situ* polymerized EDOT (PEDOT : Ts). (B) The pore-size distribution plots were obtained from a DFT-based pore-size distribution model. All the adsorption profiles in A (excluding PEDOT : Ts) are similar in shape and produce corresponding pore-size distribution plots (all centred at 2.13 nm or higher) which do not show smaller pore sizes with increased EDOT loading.

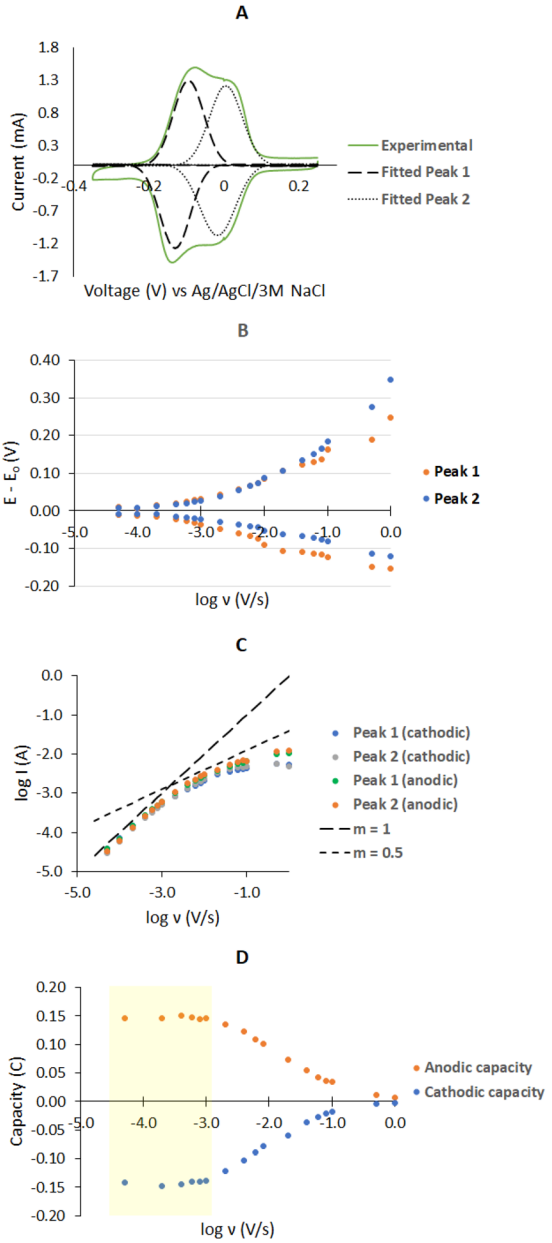

Fig. 5 Plots depicting how the electrochemical performance parameters such as half-wave potential (B), current (C), and capacity (D) changed at different scan rates for the 0.4EDOT@TpOMe-DAQ composite and evaluated assuming a two peak (with equal area) voltammetric response (A).

toluenesulfonic acid). We compared the properties of 0.4EDOT@TpOMe-DAQ with those of 0.8EDOT@TpOMe-DAQ (both composites showed an RSA of approximately 90%) to map any changes in mass transport within the material. The cyclic voltammograms obtained for 0.4EDOT@TpOMe-DAQ showed two partially separated oxidation and reduction peaks (Fig. 5A), especially at low scan rates. A similar peak splitting was previously observed for benzoquinone redox potentials when its units were coupled to a conducting polymer and measured in an acidic aqueous electrolyte.[32] As each peak was assigned to the $1e^-/1H^+$ hydroquinone-semiquinone and semiquinone-quinone steps,[32] each peak observed in the 0.4EDOT@TpOMe-DAQ voltammograms was also assumed to represent either a quinone-semiquinone or semiquinone-hydroquinone step. A scan rate study of 0.4EDOT@TpOMe-DAQ, which was evaluated by deconvoluting the voltammogram peaks (Fig. 5A), showed the half-wave potential for both steps separated at higher scan rates (Fig. 5B). From Fig. 5B–D, reasonably low $E - E_0$ values, a gradient of 1 for $\log I$ *vs.* $\log \nu$ plots and almost constant capacity, all observed for low scan rate values (ν = 0.05–1 mV s^{-1}), suggested that the material would not be well suited for fast charge–discharge applications without losing a sizeable portion of its faradaic charge capacity.[27] At scan rates above 1 mV s^{-1}, the material's capacity fell off with scan rate (Fig. 5D), and a concurrent gradient shift from 1 to 0.5 for $\log I$ *vs.* $\log \nu$ plots was observed (Fig. 5C). This gradient change from 1 (expected for surface-bound redox-active materials) to 0.5 (typical for redox-active species in solution) strongly suggests a mass-transfer limitation. We suspected

 This journal is © The Royal Society of Chemistry 2023

Open Access Article. Published on 13 April 2023. Downloaded on 7/30/2025 3:06:44 AM.
This article is licensed under a Creative Commons Attribution 3.0 Unported Licence.

that at higher scan rates, either electron diffusion or proton/counter-ion diffusion throughout the composite limited its charge storage capacity. It is also noteworthy that reliable RSA measurements require a scan rate with which the material's capacity is not limited, that is, slow scan rates in the yellow plateau region of Fig. 5D.

It should be kept in mind that electrochemical performance data can also be affected by variation in particle morphology as well as proper adhesion to the current collector as pointed out for example by Marder *et al.*[24] Adding more conducting polymer could result in better electronic conductivity while hindering ion transport, particularly if the polymer fills the COF pores. Similar scan rate studies, as described above, were also performed on the 0.8EDOT@TpOMe-DAQ composite (ESI Fig. S40‡), which showed similar mass-transport-limiting characteristics and no significant electrochemical improvements or deterioration compared to 0.4EDOT@TpOMe-DAQ. To elucidate whether the mass-transport limitations were caused by limited interparticle-electron diffusion or by proton/counter-ion diffusion, we performed similar scan rate studies on the 0.4EDOT@TpOMe-DAQ composite blended with conductive carbon PBX51 at a C : 0.4EDOT@TpOMe-DAQ mass ratio of 0.38 (ESI Fig. S31‡). The addition of PBX51 was expected to minimise any electron-transport limitations arising from poor interparticle and particle-current-collector conductivity. Again, the electrochemical performance comparison showed no improvement and pointed toward a proton/counter-ion diffusion limitation throughout the composite material or an intraparticle electron-diffusion limitation.

The redox match between anthraquinone and PEDOT was confirmed by depositing 0.4EDOT@TpOMe-DAQ with a 10% PVDF binder on gold IDA electrodes and evaluating its CV response. When using the bipotentiostat setup, a bias (0.01 V) between the working electrodes causes the currents to diverge when the material is able to conduct electrons, and the conductance can be measured. When cyclic voltammetry was performed without a proton source in acetonitrile (using 0.1 M $TBAPF_6$ electrolyte) in the voltage window −1.0 to 0.7 V (*vs.* Fc/Fc^+), only the current from the PEDOT : Ts component was visible (ESI Fig. S32‡). Under these measurement conditions, the material produced a voltammogram typical of PEDOT, demonstrated a conductance of 7.4 mS, and showed a conductance onset potential starting at −0.33 V (*vs.* Fc/Fc^+), which demonstrated it to be a functional component of the composite. For the same measurements performed in water with a 0.5 M *para*-toluenesulfonic acid acting as both the electrolyte and proton source, a maximum conductance of 7.7 mS was reached at 0.4 V (*vs.* Ag/AgCl) and it dropped to 4.0 mS at −0.3 V (*vs.* Ag/AgCl) (Fig. 6A). The PEDOT : Ts component was shown to be conductive over the anthraquinone redox-active voltage window, thus constituting a redox match. A control measurement of pristine TpOMe-DAQ with 10% PVDF (which produced RSA values of approximately 0.76%) showed a conductance value indistinguishable from that of an IDA blank (Fig. 6B). The control measurement further supports the premise that the low RSA in pristine TpOMe-DAQ is due to poor conductivity throughout the material.

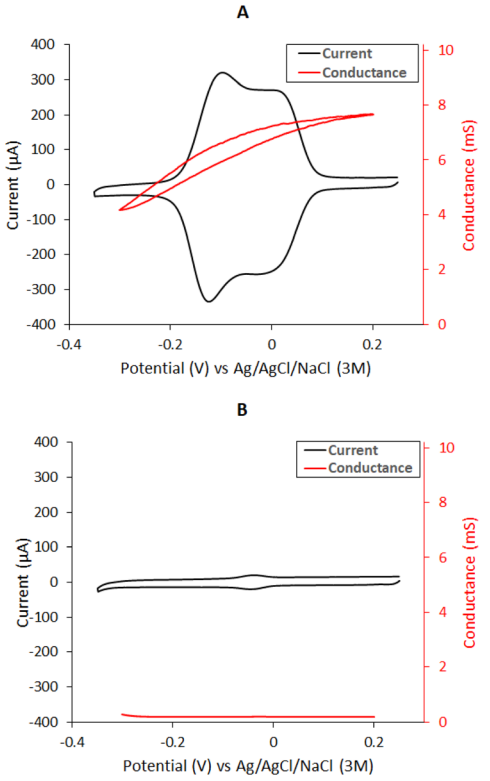

Fig. 6 *In situ* conductance plots of the 0.4EDOT@TpOMe-DAQ composite (A) and the pristine TpOMe-DAQ (B) obtained by depositing the respective materials on gold IDA electrodes and acquired in 0.5 pTSA aqueous electrolyte. The conductance in pristine TpOMe-DAQ (B) was *ca.* 1000× smaller compared to that of the 0.4EDOT@TpOMe-DAQ composite (A).

Finally, a RACOF-air secondary battery was fabricated by combining the optimised 0.4EDOT@TpOMe-DAQ composite electrode as an anode, a Pt/C catalyst cathode, and 0.5 M H_2SO_4 aqueous electrolyte (Fig. 7A and B). The battery configuration was inspired by our previous studies on polymer-air batteries.[33–36] The charge/discharge profile (Fig. 7C) showed a high discharging voltage centred between 0.8–1.2 V, which corresponded to the potential window of the 0.4EDOT@TpOMe-DAQ composite electrode when cycling it in a similar acidic electrolyte (Fig. 6A). The gravimetric capacity of the anode material (Fig. 7C) was calculated for the portion of TpOMe-DAQ in the composite, and was found to be 139 mA h g^{-1} at 1C. Compared with the theoretical gravimetric capacity of 144.7 mA h g^{-1} for pristine TpOMe-DAQ, this value suggests that the RSA of TpOMe-DAQ in the air battery was 96%, which agrees with the RSA value of 90% obtained using three-electrode cyclic voltammetry. In battery applications, especially over a 1 V window, a small capacitive and doping-charge contribution is expected to originate from the PEDOT component in the composite.[37] These contributions were minimised when RSA calculations were performed in a three-electrode setup by integrating above the capacitive background. Consequently, the slightly higher RSA value obtained for TpOMe-DAQ *via* device measurements was not unexpected. The battery,

Open Access Article. Published on 13 April 2023. Downloaded on 7/30/2025 3:06:44 AM.
This article is licensed under a Creative Commons Attribution 3.0 Unported Licence.

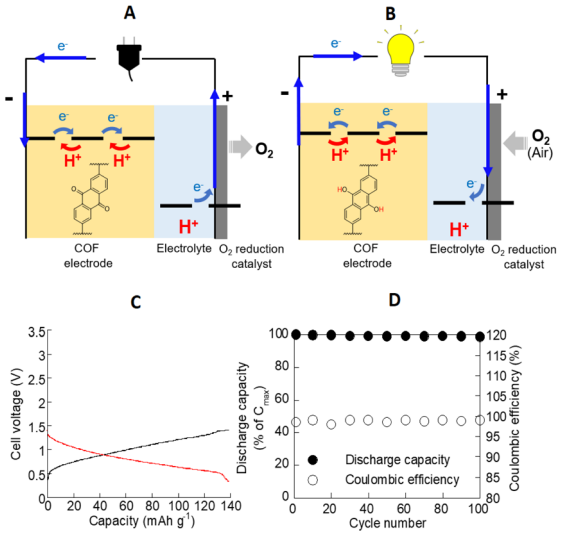

Fig. 7 Schematic of the RACOF–air secondary battery during charging (A) and discharging (B). The charging (black)/discharging (red) of the battery at 1C (C) and the stability studies and coulombic efficiency over 100 cycles (D).

together with the three-electrode-based RSA calculations, confirmed that nearly all the anthraquinone moieties (which store two electrons and two protons) in TpOMe-DAQ could be accessed. It also exhibited a high cyclability of over 99% of its initial capacity even after 100 cycles, with a high coulombic efficiency of nearly 99%. It is worth emphasizing that due to the relatively fragile electrodes and narrow potential stability window of water, these organic aqueous batteries are unlikely to effectively compete with their Li-ion counterparts for commercial applications. The exploration into alternative binders and processing methods which could increase the electrode's robustness and quality is ongoing.

Conclusions

In this study, we have shown how redox-site accessibility (RSA) can be used as an effective tool to optimise the type and amount of conductive additive needed to activate all possible redox sites in a nonconducting porous polymer, specifically a 2D RACOF. By employing *in situ*-formed PEDOT, over 90% of the redox sites were activated at a mass ratio as low as 0.3 of EDOT : TpOMe-DAQ. Increasing the loading beyond this point does not produce any detectable benefits, and only reduces the material's surface area and gravimetric capacity by adding additional weight. In addition, the electrochemical response of a material containing twice as much PEDOT as required to activate all its redox sites maintains the same performance. For functional materials that are less concerned with weight, such as sensors or electrocatalysts, loading more than the necessary conductive polymer should be explored. The significant increase in RSA associated with the *in situ* polymerisation of EDOT supports the established view that conducting polymer chains form within the pore structure and allow efficient electron transfer to and from the redox sites within the crystalline material. However, at least for TpOMe-DAQ, we could not measure any pore-size reduction or electrochemical mass-transport limitation which would be associated with pore overloading. It is possible that efficient and close polymer-COF coverage or a single polymer strand deep within the pores (which prevents further loading) could be responsible for the significant improvement in the RSA. Regardless of the cause, both the three-electrode characteristics and air-battery application of the 0.4EDOT@TpOMe-DAQ composite demonstrated that it is a functional material capable of electrochemical energy storage. This composite is best described as a battery material because almost all the anthraquinone units are utilised giving rise to a significant proportion of faradaic charge when employed as the anode in an organic-air battery.

The methods and characterisation protocols developed herein allow small amounts (1–2 mg) of redox-active COF to be screened for optimal conducting-additive addition and subsequent scale-up. We believe that this approach can serve as a general guide for the electrification and characterisation of RACOFs and is likely to be valid for other types of porous polymers. However, in order to verify this, other types of 1D, 2D and 3D materials would need to be similarly investigated in order to form a reliable structure–property relationship guide to which combination of polymer and additive gives the best electrochemical performance.

Conflicts of interest

There are no conflicts to declare.

Acknowledgements

TG, SO, and RE gratefully acknowledge Formas – a Swedish Research Council for Sustainable Development (grant number:2019-01285), the Åforsk foundation (19-352), Magnus Bergvalls stiftelse (2020-03665), and the Lars Hierta Memorial Foundation for Financial Support. This study made use of the NMR Uppsala infrastructure, which is funded by the Department of Chemistry - BMC and the Disciplinary Domain of Medicine and Pharmacy. KO acknowledges the support from Grants-in-Aid for Scientific Research (grant number 22K14732) from MEXT, Japan. KO also acknowledges support from the LNest Grant from Nipponham, FUSO Innovative Technology Fund, Masuyakinen Basic Research Foundation, and Shorai Foundation for Science and Technology. The authors thank Prof. Martin Sjödin and Assoc Prof. Ocean Cheung for valuable discussions regarding electrochemical and N_2 sorption measurements respectively.

Notes and references

1 J. W. Colson and W. R. Dichtel, *Nat. Chem.*, 2013, **5**, 453–465.
2 C. S. Diercks and O. M. Yaghi, *Sci.*, 2017, 355.
3 J. Kim, J. H. Kim and K. Ariga, *Joule*, 2017, **1**, 739–768.
4 F. Xu, S. Jin, H. Zhong, D. Wu, X. Yang, X. Chen, H. Wei, R. Fu and D. Jiang, *Sci. Rep.*, 2015, **5**, 8225.

This journal is © The Royal Society of Chemistry 2023

Open Access Article. Published on 13 April 2023. Downloaded on 7/30/2025 3:06:44 AM.
This article is licensed under a Creative Commons Attribution 3.0 Unported Licence.

5 Z. Luo, L. Liu, J. Ning, K. Lei, Y. Lu, F. Li and J. Chen, *Angew. Chem., Int. Ed.*, 2018, **57**, 9443–9446.
6 E. Vitaku, C. N. Gannett, K. L. Carpenter, L. Shen, H. D. Abruña and W. R. Dichtel, *J. Am. Chem. Soc.*, 2020, **142**, 16–20.
7 S. Wang, Q. Wang, P. Shao, Y. Han, X. Gao, L. Ma, S. Yuan, X. Ma, J. Zhou, X. Feng and B. Wang, *J. Am. Chem. Soc.*, 2017, **139**, 4258–4261.
8 H. Gao, Q. Zhu, A. R. Neale, M. Bahri, X. Wang, H. Yang, L. Liu, R. Clowes, N. D. Browning, R. S. Sprick, M. A. Little, L. J. Hardwick and A. I. Cooper, *Adv. Energy Mater.*, 2021, **11**, 2101880.
9 M. Li, J. Liu, T. Zhang, X. Song, W. Chen and L. Chen, *Small*, 2021, **17**, 2005073.
10 S. Lin, C. S. Diercks, Y.-B. Zhang, N. Kornienko, E. M. Nichols, Y. Zhao, A. R. Paris, D. Kim, P. Yang, O. M. Yaghi and C. J. Chang, *Science*, 2015, **349**, 1208–1213.
11 L. Wang, M. Deng, H. Xu, W. Li, W. Huang, N. Yan, Y. Zhou, J. Chen and Z. Qu, *ACS Appl. Mater. Interfaces*, 2020, **12**, 37619–37627.
12 Y. Li, X. Guo, X. Li, M. Zhang, Z. Jia, Y. Deng, Y. Tian, S. Li and L. Ma, *Angew. Chem., Int. Ed.*, 2020, **59**, 4168–4175.
13 C. Liang, H. Lin, Q. Wang, E. Shi, S. Zhou, F. Zhang, F. Qu and G. Zhu, *J. Hazard. Mater.*, 2020, **381**, 120983.
14 S. K. Bhardwaj, N. Bhardwaj, R. Kaur, J. Mehta, A. L. Sharma, K.-H. Kim and A. Deep, *J. Mat. Chem. A*, 2018, **6**, 14992–15009.
15 V. Venugopal, T. Hery, V. Venkatesh and V. B. Sundaresan, *J. Intell. Mater. Syst. Struct.*, 2017, **28**, 760–771.
16 C. R. Mulzer, L. Shen, R. P. Bisbey, J. R. McKone, N. Zhang, H. D. Abruña and W. R. Dichtel, *ACS Cent. Sci.*, 2016, **2**, 667–673.
17 M. S. Lohse and T. Bein, *Adv. Funct. Mater.*, 2018, **28**, 1705553.
18 C. R. DeBlase, K. E. Silberstein, T.-T. Truong, H. D. Abruña and W. R. Dichtel, *J. Am. Chem. Soc.*, 2013, **135**, 16821–16824.
19 X. Kong, S. Zhou, M. Strømme and C. Xu, *Carbon*, 2021, **171**, 248–256.
20 Y. Wu, D. Yan, Z. Zhang, M. M. Matsushita and K. Awaga, *ACS Appl. Mater. Interfaces*, 2019, **11**, 7661–7665.
21 Q. Xu, S. Dalapati and D. Jiang, *ACS Cent. Sci.*, 2016, **2**, 586–587.
22 B. Le Ouay, M. Boudot, T. Kitao, T. Yanagida, S. Kitagawa and T. Uemura, *J. Am. Chem. Soc.*, 2016, **138**, 10088–10091.
23 P. Salcedo-Abraira, A. Santiago-Portillo, P. Atienzar, P. Bordet, F. Salles, N. Guillou, E. Elkaim, H. Garcia, S. Navalon and P. Horcajada, *Dalton Trans.*, 2019, **48**, 9807–9817.
24 S. Jhulki, C. H. Feriante, R. Mysyk, A. M. Evans, A. Magasinski, A. S. Raman, K. Turcheniuk, S. Barlow, W. R. Dichtel, G. Yushin and S. R. Marder, *ACS Appl. Energy Mater.*, 2021, **4**, 350–356.
25 A. Halder, M. Ghosh, A. Khayum M, S. Bera, M. Addicoat, H. S. Sasmal, S. Karak, S. Kurungot and R. Banerjee, *J. Am. Chem. Soc.*, 2018, **140**, 10941–10945.
26 A. Halder, S. Karak, M. Addicoat, S. Bera, A. Chakraborty, S. H. Kunjattu, P. Pachfule, T. Heine and R. Banerjee, *Angew. Chem., Int. Ed.*, 2018, **57**, 5797–5802.
27 Y. Gogotsi and R. M. Penner, *ACS Nano*, 2018, **12**, 2081–2083.
28 J. Entwistle, R. Ge, K. Pardikar, R. Smith and D. Cumming, *Renewable Sustainable Energy Rev.*, 2022, **166**, 112624.
29 C. Strietzel, K. Oka, M. Strømme, R. Emanuelsson and M. Sjödin, *ACS Appl. Mater. Interfaces*, 2021, **13**, 5349–5356.
30 R. Emanuelsson, M. Sterby, M. Strømme and M. Sjödin, *J. Am. Chem. Soc.*, 2017, **139**, 4828–4834.
31 C. Strietzel, M. Sterby, H. Huang, M. Strømme, R. Emanuelsson and M. Sjödin, *Angew. Chem., Int. Ed.*, 2020, **59**, 9631–9638.
32 C. Karlsson, H. Huang, M. Strømme, A. Gogoll and M. Sjödin, *J. Electroanal. Chem.*, 2014, **735**, 95–98.
33 K. Oka, S. Furukawa, S. Murao, T. Oka, H. Nishide and K. Oyaizu, *Chem. Commun.*, 2020, **56**, 4055–4058.
34 K. Oka, S. Murao, M. Kataoka, H. Nishide and K. Oyaizu, *Macromolecules*, 2021, **54**, 4854–4859.
35 K. Oka, S. Murao, K. Kobayashi, H. Nishide and K. Oyaizu, *ACS Appl. Energy Mater.*, 2020, **3**, 12019–12024.
36 K. Oka, C. Strietzel, R. Emanuelsson, H. Nishide, K. Oyaizu, M. Strømme and M. Sjödin, *ChemSusChem*, 2020, **13**, 2280–2285.
37 L. Åkerlund, R. Emanuelsson, G. Hernández, M. Strømme and M. Sjödin, *J. Mat. Chem. A*, 2020, **8**, 12114–12123.
38 M. Thommes, K. Kaneko, A. V. Neimark, J. P. Olivier, F. Rodriguez-Reinoso, J. Rouquerol and K. S. Sing, *Pure Appl. Chem.*, 2015, **87**, 1051–1069.